

On the stark difference in satellite distributions around the Milky Way and Andromeda

Basilio Yniguez^{*}, Shea Garrison-Kimmel, Michael Boylan-Kolchin[†], James S. Bullock
Center for Cosmology, Department of Physics and Astronomy, 4129 Reines Hall, University of California, Irvine, CA 92697, USA

10 August 2018

arXiv:1305.0560v1 [astro-ph.GA] 2 May 2013

ABSTRACT

We compare spherically-averaged radial number counts of bright ($\gtrsim 10^5 L_\odot$) dwarf satellite galaxies within 400 kpc of the Milky Way (MW) and M31 and find that the MW satellites are much more centrally concentrated. Remarkably, the two satellite systems are almost identical within the central 100 kpc, while M31 satellites outnumber MW satellites by about a factor of four at deprojected distances spanning 100-400 kpc. We compare the observed distributions to those predicted for Λ CDM subhalos using a suite of 44 high-resolution $\sim 10^{12} M_\odot$ halo zoom simulations, 22 of which are in pairs like the MW and M31. We find that the radial distribution of satellites around M31 is fairly typical of those predicted for subhalos, while the Milky Way’s distribution is more centrally concentrated than *any* of our simulated Λ CDM halos. One possible explanation is that our census of *bright* ($\gtrsim 10^5 L_\odot$) MW dwarf galaxies is significantly incomplete beyond ~ 100 kpc of the Sun. If there were $\sim 8 - 20$ more bright dwarfs orbiting undetected at 100-400 kpc distance, then the Milky Way’s radial distribution would fall within the range expected from subhalo distributions and also look very much like the known M31 system. We use our simulations to demonstrate that there is enough area left unexplored by the Sloan Digital Sky Survey and its extensions that the discovery of ~ 10 new bright dwarfs is not implausible given the expected range of angular anisotropy of subhalos in the sky.

Key words: Galaxy: halo — galaxies: individual: M31 — galaxies: dwarf — Local Group

1 INTRODUCTION

The satellite galaxy populations around the Milky Way and M31 provide important laboratories for galaxy formation on small scales and benchmarks for cosmological predictions associated with dark matter halo substructure (Kravtsov 2010; Bullock 2010). Perhaps the most famous example is the Missing Satellites Problem, which points to a mismatch in the observed counts of dwarf satellites compared to the predicted number of Λ CDM dark matter subhalos that are arguably massive enough to have formed stars (Klypin et al. 1999; Moore et al. 1999). Over the last decade, discoveries of new dwarf satellite galaxies around the Milky Way in Sloan Digital Sky Survey (SDSS; York et al. 2000) data have alleviated this problem to some extent (Willman et al. 2005; Zucker et al. 2006a; Zucker et al. 2006b; Belokurov et al. 2006; Grillmair 2006; Walsh et al. 2007; Irwin et al. 2007). Specifically, a new population of *ultra-faint* dwarfs ($L \simeq 10^2 - 10^4 L_\odot$) have been discovered that that pile up along

the radial detection limit of the SDSS (Koposov et al. 2008; Walsh et al. 2009). Completeness corrections suggest that there could be as many as a few hundred *ultra-faint* dwarfs within the virial radius of the Milky Way (Tollerud et al. 2008; Walsh et al. 2009).

Given that our Galactic satellite census suffers from radially-biased incompleteness effects, M31 and its satellite system provides a particularly useful comparison set. The observational biases with M31 satellite searches are qualitatively different from those faced in Milky Way. In particular, we view M31 from the outside, yet are close enough to detect fairly low luminosity dwarf spheroidal galaxies there. The Pan-Andromeda Archeological Survey (PANdAS; McConnachie et al. 2009) provides a uniform search for dwarfs around M31, and has thus far discovered about half of the known M31 satellites. Their coverage is complete to within a projected distance of 150 kpc and outer M31 halo coverage is ongoing (Richardson et al. 2011). Interestingly, the current M31 dwarf count, which is almost certainly incomplete beyond 150 kpc, is larger than the Milky Way count by about a factor of two at fixed luminosity (see below). This difference is striking given that

^{*} email: byniguez@uci.edu

[†] Center for Galaxy Evolution Fellow

the two spirals have the same luminosity to within $\sim 30\%$ (van den Bergh et al. 2000).

Beyond the question of overall counts, another useful comparison concerns the relative radial distribution of satellite galaxies. The Milky Way satellites are known to be more centrally concentrated around the Galaxy than would be expected for subhalos in dissipationless Λ CDM simulations (Moore 2001; Willman et al. 2004; Macciò et al. 2010). This basic mismatch has been used as a potential testing ground for ideas to solve the Missing Satellites Problem. For example, early-forming halos that formed before reionization tend to be more centrally concentrated than the overall population (Bullock et al. 2000; Moore 2001). The problem with this explanation is that the mismatch between naive theory and observation appears to be much less severe for M31.

Willman et al. (2004) were the first to emphasize that known M31 satellite galaxy population was somewhat more extended than that of the Milky Way, and suggested that the disagreement could be explained by incompleteness in the outer Milky Way halo, possibly as a result of the difficulty in detecting low-surface brightness systems at low Galactic latitude. Importantly, at the time of their work, all of the known satellites of M31 and the Milky Way were “bright” by today’s standards, with luminosities $L > 10^5 L_\odot$. They emphasized that this possible incompleteness in (bright) satellites provided motivation for searches for new dwarfs via resolved-stars in the Sloan Digital Sky Survey. As already mentioned, these searches have proven immensely successful at finding new *faint* dwarfs, but new bright dwarfs of the type known before 2004 have remained sparse: all but one of the ~ 15 new dwarfs that have been discovered since 2004 are less luminous than $10^5 L_\odot$ and none are more luminous than $3 \times 10^5 L_\odot$. Over the same period, 20 new M31 satellite galaxies have been discovered, 14 of which are *more* luminous than $10^5 L_\odot$.

In this paper we reexamine the radial distributions of M31 satellites and Milky Way satellites. We restrict ourselves to the brightest systems: bright enough that we could possibly assume our census of them complete within the Milky Way virial radius. Given the new discoveries of mainly bright satellites around M31, we expect to see the difference in their radial populations to be even more discrepant than previously quantified (McConnachie 2006). This discrepancy may grow yet with the discovery of additional satellites around M31 as PAndAS coverage expands (Richardson et al. 2011).

The outline of this paper is as follows: in Section 2 we describe the data sets of the MW, M31 and our suite of Λ CDM simulations. Section 3 contains the results of our comparison, Section 4 discusses the possible effects of incompleteness in the satellite populations and in Section 5 we conclude.

2 DATA

2.1 Satellites of the MW and M31

The M31 and Milky Way satellite data sets we examine in this paper are summarized in Table 1, with data taken from the review by McConnachie (2012). Galaxies are listed in

the order they were found in order to emphasize the great explosion of discoveries in the post SDSS/PAndAS era (horizontal break). We include only systems that could be within 400 kpc physical separation of each host, given published distance uncertainties.

The Milky Way satellites listed in Table 1 are restricted to those brighter than the faintest known M31 dwarfs ($> 10^4 L_\odot$), 15 in all. Twelve of these are brighter than $10^5 L_\odot$, the approximate completeness limit of SDSS at 400 kpc and of PAndAS for M31 satellite discovery (Richardson et al. 2011). Only one of the new dwarfs discovered in the $\sim 1/3$ of the sky covered by the SDSS is brighter than this: Canes Venatici I at 220 kpc distance. This has provided some motivation for assuming that the Milky Way census of *bright* dwarfs is reasonably complete out to the virial extent of the Milky Way (~ 300 kpc), though it will be impossible to quantify this completeness with certainty until uniform, full-sky, resolved-star searches have been completed.

The M31 data set includes a total of 32 galaxies, more than half of which were discovered in the last six years. The census of dwarfs in the vicinity of M31 is well-understood within a projected radius of about 150 kpc of the M31 center (Richardson et al. 2011). Although the faintest known M31 dwarfs known have luminosities down to $\sim 10^4 L_\odot$, the PAndAS survey’s limit for efficient detection is closer to $L_V \sim 10^5 L_\odot$ (Richardson et al. 2011). This completeness limit applies only to the region within 150 kpc of the M31 disk. Of the 32 M31 satellites listed, 26 are brighter than $10^5 L_\odot$. We will use this luminosity as a characteristic luminosity for comparison in this work. We have not included And VIII and And XVIII in our comparison set. Merrett et al. (2006) have questioned And VIII’s classification as a galaxy because of tidal features. And XVIII has a very high deprojected separation from the center of M31, falling outside of our 400 kpc region of consideration.

The deprojected distances and errors in Table 1 were derived from the heliocentric distances and errors quoted in McConnachie (2012). The separation between M31 and one of its satellites is given by

$$r_{M31} = \sqrt{R^2 + d^2 - 2Rd \cos \theta}, \quad (1)$$

where R is the heliocentric distance of M31, d is the heliocentric distance of the satellite and θ is the angular separation between the two. We sampled the heliocentric distance of M31 and of each satellite 1000 times, drawing from a Gaussian based on quoted line-of-sight errors to obtain the error limits of r_{M31} , which are not always Gaussian-like themselves.

2.2 Simulations

We use a total of 44 Milky-Way size halos simulated as part of the ELVIS project, which is described in detail in Garrison-Kimmel et al. (in preparation); here we summarize the relevant properties. ELVIS is a suite of collisionless zoom-in simulations designed to study the Local Group. It consists of twenty-two halos in paired systems that were chosen to resemble the M31 and Milky Way in mass and phase-space configuration in addition to twenty-two halos that are isolated, mass-matched analogues, which serve as a control sample to examine any trends due to the paired nature of the Local Group system. The host dark matter halos have

Name	d_{M31} [kpc]	$L_V [L_\odot]$	Discovered	Name	d_{MW} [kpc]	$L_V [L_\odot]$	Discovered
M31	-	2.6×10^{10}	-	Milky Way	-	2.0×10^{10}	-
M32	23^{+45}_{-17}	2.9×10^8	1749	LMC	49 ± 3	2.2×10^9	-
M33	209^{+7}_{-5}	2.8×10^9	1764	SMC	58 ± 4	5.9×10^8	-
NGC205	42^{+27}_{-25}	3.7×10^8	1783	Sculptor	79 ± 4	7.1×10^5	1937
NGC185	185^{+16}_{-16}	1.8×10^8	1787	Fornax	140 ± 8	1.5×10^7	1938
NGC147	120^{+11}_{-10}	1.4×10^8	1829	LeoI	254 ± 30	4.9×10^6	1950
IC10	252^{+11}_{-5}	8.6×10^7	1888	LeoII	208 ± 12	9.4×10^5	1950
AndI	71^{+14}_{-13}	4.5×10^6	1971	Ursa Minor	68 ± 3	2.8×10^5	1954
AndII	198^{+11}_{-10}	9.4×10^6	1974	Draco	76 ± 5	2.8×10^5	1954
AndIII	88^{+17}_{-10}	1.0×10^6	1974	Carina	103 ± 5	4.9×10^5	1977
Pisces	268^{+4}_{-2}	9.4×10^5	1976	Sextans	89 ± 4	5.4×10^5	1990
AndV	115^{+8}_{-4}	7.1×10^5	1998	Sagittarius	20 ± 4	8.6×10^7	1994
AndVI	269^{+5}_{-3}	3.4×10^6	1999				
AndVII	219^{+5}_{-0}	1.8×10^7	1999				
AndIX	186^{+23}_{-87}	$1. \times 10^5$	2004	Ursa Major I	105 ± 10	1.4×10^4	2005
AndX	126^{+33}_{-18}	1.5×10^5	2006	Bootes I	64 ± 6	2.8×10^4	2006
AndXI	103^{+54}_{-1}	4.9×10^4	2006	Hercules	145 ± 13	3.7×10^4	2006
AndXII	178^{+35}_{-73}	3.1×10^4	2006	Canes Ven. I	220 ± 20	2.4×10^5	2006
AndXIII	116^{+88}_{-1}	4.1×10^4	2006				
AndXIV	161^{+59}_{-2}	1.8×10^5	2007				
AndXV	178^{+31}_{-60}	4.9×10^5	2007				
AndXVI	323^{+27}_{-40}	4.1×10^5	2007				
AndXVII	70^{+24}_{-23}	2.1×10^5	2008				
AndXIX	114^{+33}_{-9}	4.5×10^5	2008				
AndXX	130^{+21}_{-4}	2.8×10^4	2008				
AndXXI	134^{+11}_{-8}	7.8×10^5	2009				
AndXXII	270^{+21}_{-56}	5.4×10^4	2009				
AndXXIII	129^{+6}_{-2}	1.0×10^6	2011				
AndXXIV	166^{+22}_{-28}	9.4×10^5	2011				
AndXXV	93^{+46}_{-8}	6.5×10^5	2011				
AndXXVI	104^{+116}_{-2}	5.9×10^4	2011				
AndXXVII	478^{+41}_{-420}	1.2×10^5	2011				
AndXXVIII	369^{+17}_{-2}	2.1×10^5	2011				
AndXXIX	188^{+25}_{-3}	1.8×10^5	2011				

Table 1. Satellite galaxies of M31 (left) and Milky Way (right) used in this work, listed in order of their discovery date. The horizontal band marks the transition from the “classical” era of discovery to the post-SDSS/PAndAS era. With a deprojected distance greater than 400 kpc (with relatively small uncertainty), And XVIII may not be a bound satellite of M31; it is therefore not listed here or included in any figures. For completeness, we list all satellites brighter than $L_V = 10^4 L_\odot$ here, though we only present data for systems fainter than $L_V = 10^5 L_\odot$ in Figure 1. We use the more conservative cut at $L_V = 10^5 L_\odot$ for subsequent figures and radial comparisons. Luminosities are taken from Watkins et al. (2012) and McConnachie (2012) while the host-satellite separations and associated errors were computed from the heliocentric distances quoted by those authors.

virial masses between $1.0 - 2.8 \times 10^{12} M_\odot$ and associated virial radii $R_{\text{vir}} = 265 - 370$ kpc, with maximum circular velocities that range from $V_{\text{max}} = 155 - 225 \text{ km s}^{-1}$.

All ELVIS halos were simulated in a Λ CDM cosmology with parameters based on WMAP7 results (Larson et al. 2011): $\sigma_8 = 0.801$, $\Omega_m = 0.266$, $\Omega_\Lambda = 0.734$, $n_s = 0.963$, and $h = 0.71$. The simulations were run with identical mass resolution (particle mass $m_p = 1.9 \times 10^5 M_\odot$); likewise, all simulations were run with a Plummer-equivalent force softening of 140 pc, which was comoving until $z = 9$, after which a physical softening length was imposed. All simulations are uncontaminated by low-resolution particles to at least 900

kpc from the center of each host. Halo substructure was identified with **Rockstar** (Behroozi et al. 2012a), and merger trees were built using **consistent-trees** (Behroozi et al. 2012b). At this resolution, we are complete to subhalos with current maximum circular velocity $V_{\text{max}} > 8 \text{ km s}^{-1}$ and to those with $V_{\text{peak}} > 10 \text{ km s}^{-1}$, where V_{peak} is the largest circular velocity ever achieved by the main branch of a subhalo progenitor.

Additionally, two of our host isolated halos were resimulated at an even higher resolution with a particle mass of $m_p = 2.35 \times 10^4 M_\odot$ and a force resolution of 70 pc, comparable to the resolution of the level 2 Aquarius simula-

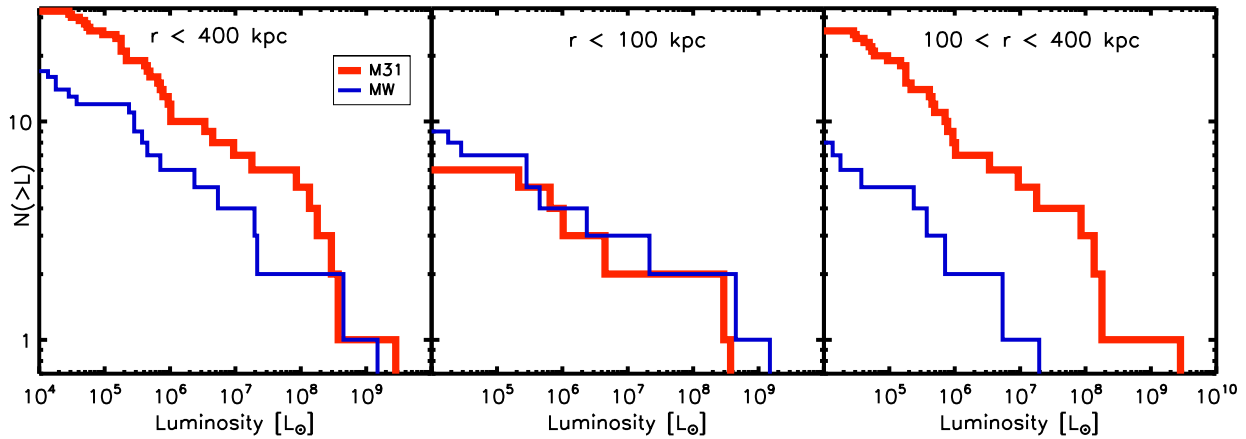


Figure 1. Satellite galaxy luminosity functions of the MW (blue) and M31 (red) for all galaxies within 400 kpc of either host (left); those within 100 kpc of either host (middle); and those in the radial range 100-400 kpc (right). While the luminosity functions within 100 kpc are very similar, M31 has approximately four times as many satellites at fixed luminosity in the 100-400 kpc range.

tions (Springel et al. 2008) and the Via Lactea I simulation (Diemand et al. 2007). The velocity functions and radial distributions of the two higher resolution host halos are nearly identical to those of the lower resolution counterparts to V_{peak} values well below those used for selecting subhalos in this work.

In our fiducial radial distribution comparisons, we select the 30 subhalos with the highest V_{peak} within 400 kpc of each host. This choice is motivated by the fact that M31 has approximately 30 satellite galaxies within this radius; this is also the approximate distance to which SDSS is complete to $L > 10^5 L_{\odot}$ dwarfs. In practice, this amounts to selecting halos with V_{peak} values greater than 20 km s^{-1} to 33 km s^{-1} , depending on the host. The overall shapes of the distributions are fairly insensitive to this specific choice. For example, when we chose the 100 most massive subhalos, or when we use a fixed V_{peak} cut, we find that the radial distributions of subhalos do not change significantly. In the Appendix, we explore the spatial distributions of subhalos with the 30 largest values of V_{max} and those with the 30 largest values of z_{peak} (the redshift at which V_{peak} is attained). For the latter case, we restrict ourselves to subhalos with $V_{\text{max}} > 10 \text{ km s}^{-1}$.

3 RESULTS

3.1 The MW and M31 satellite systems compared

The satellite luminosity functions of the MW and M31 are shown in Figure 1. The left panel includes all satellites within a deprojected radius of 400 kpc of either host.¹ Considering this full sample, M31 has approximately a factor of two more satellites at fixed luminosity. Intriguingly, however, the two systems have luminosity functions that are essentially identical when only satellites within 100 kpc are considered (middle panel). The difference in satellite luminosity functions between the two systems is entirely attributable to differences at large radial separations (100 - 400 kpc), as

shown in the right panel of Figure 1. While M31 has approximately 20 satellites brighter than $10^5 L_{\odot}$ in this radial range, the Milky Way has only 5. We note, however, that the shape of the luminosity function remains very similar at these large radii, even though the amplitude differs by a factor of ~ 4 .

A complementary demonstration of the difference between the satellite systems of the two Local Group giants is given in Figure 2, which compares the cumulative radial count of satellites brighter than $10^5 L_{\odot}$ around each host. Solid lines show median distributions and the dashed lines show 68% uncertainties derived using Monte Carlo realizations of the deprojected distances and errors listed in Table 1. M31’s satellite population is significantly more extended than that of the MW, almost entirely due to differences at $> 100 \text{ kpc}$.

In the context of observational completeness, it is remarkable that M31 has so many more satellites at a large galactocentric distances. PAndAS has provided a uniform search for (bright) dwarf galaxies only within a projected distance of 150 kpc of the Andromeda galaxy (Richardson et al. 2011), so it would not be surprising if there are even more M31 dwarfs waiting to be discovered beyond 150 kpc – a region marked by the vertical dashed line in Figure 2. Any such discoveries would only enhance the discrepancy between the MW and M31.

One way the difference in cumulative radial distributions might be reconciled is if our M31 census were incomplete at *small* projected radius, perhaps because of the difficulty in detecting low surface brightness dwarfs in the vicinity of M31’s disk. Interestingly, of the M31 dwarfs less luminous than $10^6 L_{\odot}$, And IX is the closest at a projected distance of $R = 36 \text{ kpc}$. Meanwhile, there are 2 (or 3, if And VIII is included) very luminous satellites that are within this radius. If there were a few more low-luminosity dwarfs hiding in glare of the M31 disk, this would act to shift the M31 satellite distribution towards a more concentrated shape, more in line with that of the MW. However, discoveries of this kind would further exacerbate the overall difference in *normalization* between the two satellite luminosity functions. Moreover, additional small-R discoveries around M31 would also drive the M31 radial distribution away from the

¹ In this figure we have used the best-fit radial distances of satellites listed in Table 1.

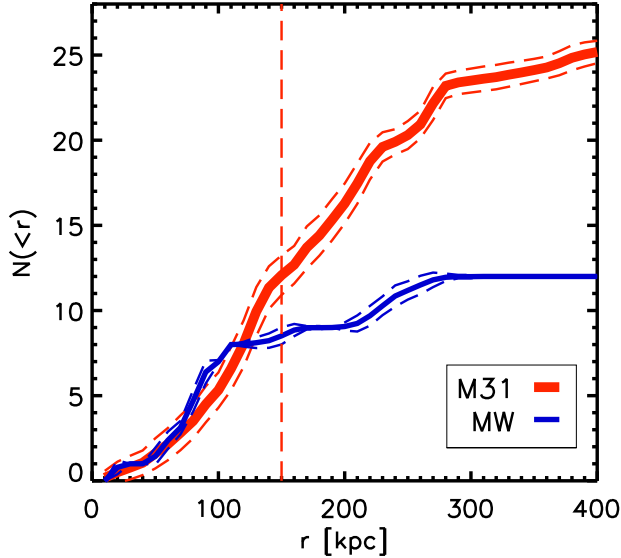


Figure 2. Cumulative number of satellites with $L > 10^5 L_\odot$ within a deprojected distance r from either the MW or M31. The solid and dashed lines show the median and 68% confidence intervals implied by current observational uncertainties. The spatial distributions are similar within ~ 100 kpc, while the M31 satellite system is significantly more extended than that of the MW outside of this radius. This is in spite of the fact that the M31 system is almost certainly incomplete at distances on the right of the vertical dashed line, which marks the edge of the region within which the PAndAS project has provided a uniform search for M31 dwarfs.

expectations for subhalos derived from our Λ CDM simulations. As we demonstrate in the next section, the distribution of presently-known M31 satellites is much more in line with subhalo distributions derived from our LCDM simulations than the known satellite distribution around the Milky Way.

3.2 Comparison to Simulations

Since the Milky Way and M31 have such different radial distributions of satellites, it is natural to ask which (if either) is more in line with theoretical expectations. We expect a correspondence between subhalos with large values of V_{peak} and luminous satellites (e.g., Bullock 2010; Kravtsov 2010). Figure 3 therefore compares the observed radial distributions of satellites of the MW (blue) and M31 (red) to those of the 30 top V_{peak} subhalos from our 44 Λ CDM simulation (gray lines); for each data set, the radial profile is normalized to the cumulative count within 100 kpc. As in Figure 2, the dashed colored lines show uncertainties associated with deprojection for the observational data.

Although there is significant scatter in the number of satellites at large radii ($\gtrsim 300$ kpc) in the simulations, it is clear that the M31 system is consistent with the profiles expected from subhalo distributions while the MW is more centrally concentrated than any of the simulated systems. A typical simulated halo has 4-5 times as many satellites

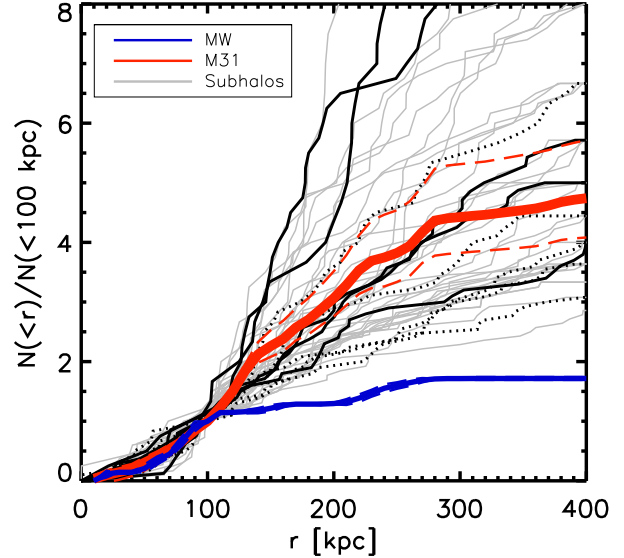


Figure 3. The cumulative number of satellites within radius r , normalized to the count within $r = 100$ kpc separation. The solid (dashed) blue and red lines show the median (68% spread) profiles for the MW and M31 satellite systems while the grey and black lines show the profiles of subhalo distributions derived from 44 Λ CDM simulations. The subhalo distributions were made from the 30 subhalos with the highest V_{peak} from each simulation. The Milky Way’s distribution is more centrally concentrated than any of the simulated systems, while M31 looks fairly typical. For reference, the five solid black lines show subhalo profiles for the five highest virial mass halos in our sample ($2.7 - 2.8 \times 10^{12} M_\odot$) and the black dotted lines are from our five lowest mass halos ($1.0 - 1.2 \times 10^{12} M_\odot$). While there is some tendency for the highest mass systems to have more extended distributions (when measured this way), the correlation is weak and shows substantial scatter.

within 300 kpc as within 100 kpc, while the corresponding number for the Milky Way is only 1.5.

The solid (dotted) black lines in the Figure correspond to the five highest (lowest) mass host halos in our sample. While two of the five most massive halos also have subhalo populations that are among the most extended of our sample, as might be expected based on their large virial radii, three of the five most massive hosts have subhalo populations that are either fairly typical or even somewhat more concentrated than average. Any trend with host halo mass is fairly weak and is overwhelmed by scatter at fixed mass (this was also seen by Wang et al. 2013).

It is useful to have a parameterization of the degree of concentration of a halo’s satellite population. For this we define a parameter B_{400} to be the ratio of the number of satellites within 400 kpc to the number within 100 kpc:

$$B_{400} \equiv N(< 400 \text{ kpc})/N(< 100 \text{ kpc}). \quad (2)$$

B_{400} is then a measure of the “puffiness” of the subhalo population. The distribution of B_{400} values for all of our simulated host systems is shown by the solid histogram in Figure 4, while the measured values for the MW and M31 are indicated by arrows. As expected, we see that the satellite distribution of the MW is more concentrated than *any*

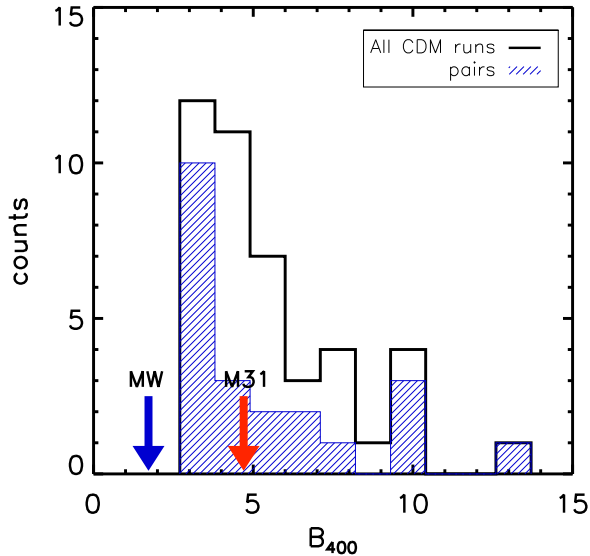


Figure 4. The distribution of subhalo radial distribution shapes — $B_{400} \equiv N(< 400\text{kpc})/N(< 100\text{kpc})$ — for all of our simulated halos (solid line) with the observed values for the MW and M31 indicated by arrows. The shaded histogram shows the subset of simulated halos that are in Local Group like pairs. The MW is clearly an outlier from the simulated distributions in that its satellite galaxy population is much more concentrated; M31 is more typical of the simulated systems.

of the simulated subhalo systems, while M31 is fairly typical of what is seen in the simulations. The shaded blue histogram shows the subset of our simulated halos that are paired, Local Group analogs; these halos are fairly similar to the isolated, mass-matched analogs in their B_{400} distributions. As a result, the fact that M31 and the MW are paired should not significantly skew their satellite radial distributions compared to field systems (at least when spherically averaged; we will explore angular anisotropy in more detail in a future paper).

Even though the MW is an outlier relative to all of our simulated systems, one might posit that the high concentration of the Milky Way’s satellite population is attributable to some physical process. However, we were unable to find any correlation between B_{400} and halo concentration, mass accretion history, or virial mass. In the Appendix, we show explicitly that the radial subhalo distributions are not tightly correlated with the bulk infall time distributions of satellites. Given that we are unable to provide a natural explanation for why the MW system is highly anomalous compared to predicted subhalo distributions (while M31 is not), in the next section we explore the possibility that the census of bright MW satellites may be incomplete at radii beyond 100 kpc.

In the Appendix we explore a few other options for selecting subhalos and the associated implications for radial distribution. For most reasonable choices, the selection on V_{peak} we use for our fiducial analysis produces a more centrally concentrated subhalo distribution than those with the highest V_{max} . However, we show that by sub-selecting $V_{\text{max}} > 10 \text{ km s}^{-1}$ subhalos that reach their V_{peak} values the

earliest (i.e. were accreted into the host halo the earliest) we can produce subhalo distributions that are more centrally concentrated (see also Wang et al. 2013), and more in line with the observed radial distribution of the Milky Way. However, this model is not very well motivated as a physical selector for luminous subhalos. As shown in the Appendix, it effectively picks out $\sim 10\%$ of the subhalos that have $V_{\text{peak}} < 30 \text{ km s}^{-1}$, and ignores an equal number of systems with $V_{\text{peak}} > 30 \text{ km s}^{-1}$. There is no astrophysical reason to expect these most massive progenitors to be dark.

3.3 Are there undiscovered bright satellites around the Milky Way?

The Milky Way satellite census may still be incomplete at large radii, even to satellites similar in luminosity to the classical dwarfs ($L > 10^5 L_{\odot}$). The only truly uniform survey with well-understood completeness limits is SDSS/SEGUE, which has covered approximately 1/3 of the sky. One bright dwarf ($L > 10^5 L_{\odot}$), Canes Venatici I, was discovered in this area (Zucker et al. 2006b). Is it therefore worthwhile to ask the question: how many new Milky Way dwarfs could plausibly be undiscovered? We investigate this question first in terms of sky coverage and angular anisotropy, then in terms of radial distributions.

Of the bright MW satellites, there are 6 that lie inside of the SDSS footprint. We can be confident that our census is complete within this region. Given this, we can provide a rough estimate for a plausible number of bright dwarfs that could exist outside this footprint using our simulations. Specifically, for each of our 44 systems, we count subhalos in randomly-oriented angular cones the size of the DR8 footprint (14555 deg^2) with a depth of 400 kpc. We determine a V_{peak} cut that yields 6 subhalos within this region. We then determine the total number of subhalos over the whole sky with V_{peak} higher than the cut. This gives the total expected number of bright satellites within a spherical region of 400 kpc, N_{expected} , based only on the count within an SDSS area.

For each host halo, we perform 10^4 random realizations of mock pointings to derive an N_{expected} distribution based on our full sample. The results are shown in Figure 5. The median prediction is 18 bright satellites over the whole sky. This can be compared to the 12 known bright MW satellites, so it is not implausible to think that ~ 6 undiscovered bright satellites of the Milky Way could be out there. In fact, the distribution extends to at total ~ 40 satellites, which would correspond to a total of ~ 28 undiscovered satellites.

How many satellites would need to be discovered beyond 100 kpc if the MW satellite distribution were to match the expectations of our Λ CDM simulations? The Milky Way has 7 bright satellites within 100 kpc, so for each of our simulated halos, the value of B_{400} can be used to compute the total number of bright MW satellites expected based on the known number within 100 kpc:

$$N_{\text{expected}} = N_{\text{MW}}(< 100 \text{ kpc}) \times B_{400} = 7 B_{400}. \quad (3)$$

The right panel of Figure 5 shows that this predicts that there would need to be a total of 20 to 40 bright MW satellites, substantially more than the 12 that have been discovered so far. The implication is that there would need to be between $\sim 8 - 28$ new satellites beyond 100 kpc in order for

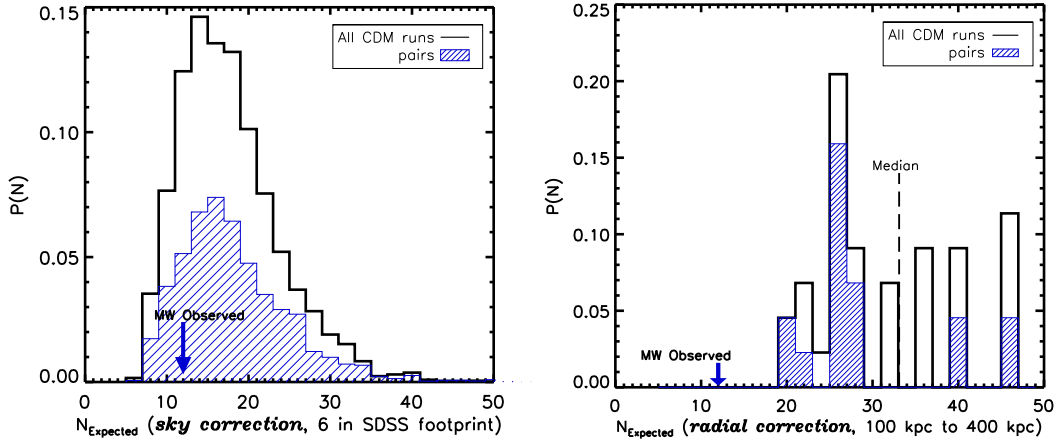


Figure 5. *Left:* The total number of Milky Way satellites expected over the whole sky given the observation that there are 6 bright satellites in the SDSS footprint (14555 deg^2). The calculation uses subhalos in our Λ CDM simulations to correct for areal incompleteness, allowing for anisotropy. The assumption is that only the SDSS area is known with confidence to be complete to systems with $L \sim 10^5 L_\odot$. *Right:* The total number of satellite galaxies expected with 400 kpc of the MW, estimated from the number of MW satellites known within 100 kpc and then assuming that ratio of satellites within 400 kpc to those with 100 kpc matches the expectation for Λ CDM subhalos (see text). The shaded regions represent the contribution due to the paired “Local Group-like” simulations. The blue arrows indicate the number of known MW satellites brighter than $10^5 L_\odot$.

the Milky Way to fall within the range of our simulations. Interestingly, this number overlaps with the allowed range from the angular coverage correction discussed above (and in the left panel of Figure 5).

To have escaped previous detection, a bright satellite would likely need to have a large half-light radius ($\sim 1 \text{ kpc}$) and low surface brightness. Canes Venatici I, the bright satellite discovered in SDSS, does indeed have such characteristics: its central surface brightness is $\mu = 27.1 \text{ mag/arcsec}^2$ and its projected half light radius is 560 pc (Zucker et al. 2006b; McConnachie 2012).

4 DISCUSSION AND CONCLUSIONS

The results of Section 3 show that the satellites of Milky Way and M31 have very different radial distributions. Within 100 kpc of their respective hosts, the $L > 10^5 L_\odot$ satellite galaxy populations of the two galaxies have similar radial distributions and luminosity functions, whereas between 100 and 400 kpc, M31 has approximately four times as many satellites as the Milky Way. While Λ CDM simulations predict substantial scatter in the radial distribution of subhalos, the MW’s satellite population is more concentrated than *all* of the simulations we have investigated. This result holds for reasonable associations between subhalos and galaxies, though extreme subsets of subhalos, chosen on formation time, can alter this conclusion (see below). M31, on the other hand, looks fairly typical when compared to the simulations.

It is possible that the Milky Way is simply an outlier in terms of the spatial distribution of its satellites - though it would need to be extreme enough to be rarer than one out of the 44 systems we have simulated. A more intriguing possibility is that the census of Milky Way satellites is incomplete not just for the faintest dwarfs, but also for brighter systems ($L \sim 10^5 L_\odot$). The discovery of Canes Venatici I by

Zucker et al. (2006b) in SDSS data indicates that this is indeed a distinct possibility. Using the distribution of subhalos from our simulations, we might expect 8-20 additional satellites if the radial distribution of the MW satellites is similar to those of subhalos in our simulations. We showed that the angular anisotropy of subhalos in our simulations allow for the possibility of 8-20 additional satellites in the area of the sky not yet surveyed for new dwarfs by the SDSS.

If the shape of the radial distributions of subhalos is a template for the radial distribution of satellite galaxies about their host, then the Milky Way almost certainly has new bright satellites yet to be discovered. This would be consistent with the expectations of hydrodynamical simulations of Bovill & Ricotti (2011) who have argued that there should be more bright satellites around the Milky Way based on their models. While the simulations we have used for our comparison are dissipationless, including baryonic physics is likely to exacerbate the discrepancy between the predicted and observed distribution of satellites in the Milky Way, as the MW disk can deplete substructure that pass nearby (D’Onghia et al. 2010).

One way to increase the predicted concentration of the MW satellite population, and therefore to bring the MW into better agreement with dissipationless Λ CDM simulations, is to associate the Milky Way’s bright satellites with its earliest forming subhalos having $V_{\text{peak}} > 10 \text{ km s}^{-1}$. Such an association also predicts that the Milky Way’s bright dwarf spheroidals (1) formed in halos with $V_{\text{peak}} \lesssim 30 \text{ km s}^{-1}$ and (2) reside in halos that currently have $V_{\text{max}} \lesssim 20 \text{ km s}^{-1}$. This scenario would be in agreement with the values derived by Boylan-Kolchin et al. (2011) based on kinematics of the MW’s bright satellites. In this case, there would be 20-40 dark matter satellites of the Milky Way that are more massive but less luminous than its bright dwarf spheroidal galaxies. This scenario is highly unnatural in current models of galaxy formation.

Although we do not see a significant difference in the subhalo radial distributions between paired and non-paired host halos, we can not rule out the possibility that the evolutions of the Milky Way and M31 are coupled in some way. The asymmetrical 3D distribution of M31's satellites (Conn et al. 2013) may hint at such a connection. We are currently using the ELVIS suite to evaluate the frequency of such “great plane” configurations in Λ CDM simulations.

ACKNOWLEDGEMENTS

Support for this work was provided by NASA through a grant for program AR-12836 from the Space Telescope Science Institute (STScI), which is operated by the Association of Universities for Research in Astronomy (AURA), Inc., under NASA contract NAS5-26555. MB-K acknowledges support from the Southern California Center for Galaxy Evolution and the UC High Performance Astro-Computing Center, multi-campus research programs funded by the University of California Office of Research. Initial calculations leading to this work was partially supported by HST-GO-12273.03-A. BY was supported by NSF grant AST-1009973. SG-K was supported by NSF grant AST-1009999.

REFERENCES

- Behroozi, P., Wechsler, R., & Wu, H.-Y. 2012, *Astrophysics Source Code Library*, 10008
- Behroozi, P. S., Wechsler, R. H., Wu, H.-Y., et al. 2012, *Astrophysics Source Code Library*, 10011
- Belokurov, V., Zucker, D. B., Evans, N. W., et al. 2006, *ApJ*, 647, L111
- Bovill, M. S., Ricotti, M. 2011, *ApJ*, 741, 18
- Bovy, J., Allende Prieto, C., Beers, T. C., et al. 2012, *ApJ*, 759, 131
- Boylan-Kolchin, M., Bullock, J. S., & Kaplinghat, M. 2011, *MNRAS*, 415, L40
- Boylan-Kolchin, M., Bullock, J. S., Sohn, S. T., Besla, G., van der Marel, R. P. 2013, *ApJ*, 768, 140
- Bullock, J. S., Kravtsov, A. V., & Weinberg, D. H. 2000, *ApJ*, 539, 517
- Bullock, J. S., Kolatt, T. S., Sigad, Y., et al. 2001, *MNRAS*, 321, 559
- Bullock, J. S. 2010, arXiv:1009.4505
- Conn, A.R., Lewis, G. F., Ibata, R. A., et al. 2013, arXiv:1301.7131
- Diemand, J., Kuhlen, M., & Madau, P. 2007, *ApJ*, 657, 262
- D’Onghia, E., Springel, V., Hernquist, L., & Keres, D. 2010, *ApJ*, 709, 1138
- Grillmair, C. J. 2006, *ApJ*, 645, L37
- Irwin, M. J., Belokurov, V., Evans, N. W., et al. 2007, *ApJ*, 656, L13
- Kafle, P. R., Sharma, S., Lewis, G. F., Bland-Hawthorn, J., 2012, *ApJ*, 761, 98
- Klypin, A., Kravtsov, A., Valenzuela, O., Prada, F., 1999, *ApJ*, 522, 82
- Koposov, S., Belokurov, V., Evans, N. W., et al. 2008, *ApJ*, 686, 279
- Kravtsov, Andrey, V., Gnedin, Oleg, Y., Klypin, Anatoly, A., 2004, *ApJ*, 609, 482
- Kravtsov, A. 2010, *Advances in Astronomy*, 2010
- Larson, D., Dunkley, J., Hinshaw, G., et al. 2011, *ApJS*, 192, 16
- Macciò, A. V., Kang, X., Fontanot, F., et al. 2010, *MNRAS*, 402, 1995
- Madau, P., Diemand, J., & Kuhlen, M. 2008, *ApJ*, 679, 1260
- McConnachie, A. W., Irwin, M. J., 2006, *MNRAS*, 365, 1263
- McConnachie, A. W., Irwin, M. J., Ibata, R. A., et al. 2009, *Nature*, 461, 66
- McConnachie, A. W., 2012, *AJ*, 144, 4
- Merrett, H. R., Merrifield, M. R., Douglas, N. G., et al. 2006, *MNRAS*, 369, 120
- Moore, B. 2001, 20th Texas Symposium on relativistic astrophysics, 586, 73
- Moore, B., Ghigna, S., Governato, F., Lake, G., Quinn, T., Stadel, J., Tozzi, P. 1999, *ApJ*, 524, L19
- Navarro, J. F., Frenk, C. S., & White, S. D. M. 1997, *ApJ*, 490, 493
- Richardson, J, Irwin, M., McConnachie, A., et al. 2011, arXiv1102.2902
- Springel, V., Wang, J., Vogelsberger, M., et al. 2008, *MNRAS*, 391, 1685
- Tollerud, E. J., Bullock, J. S., Strigari, L. E., & Willman, B. 2008, *ApJ*, 688, 277
- van den Bergh, S. 2000, *PASP*, 112, 529
- Walsh, S. M., Jerjen, H., & Willman, B. 2007, *ApJ*, 662, L83
- Walsh, S. M., Willman, B., & Jerjen, H. 2009, *AJ*, 137, 450
- Wang, J., Frenk, C. S., & Cooper, A. P. 2013, *MNRAS*, 429, 1502
- Watkins, L., Evans, N.W., van de Ven, G., 2012, arXiv1211.2638
- Willman, B., Governato, F., Dalcanton, J. J., Reed, D., & Quinn, T. 2004, *MNRAS*, 353, 639
- Willman, B., Blanton, M. R., West, A. A., et al. 2005, *AJ*, 129, 2692
- Xue, X. X., Rix, H. W., Zhao, G., et al. 2008, *ApJ*, 684, 1143
- York, D. G., Adelman, J., Anderson, J. E., Jr., et al. 2000, *AJ*, 120, 1579
- Zucker, D. B., Belokurov, V., Evans, N. W., et al. 2006, *ApJ*, 650, L41
- Zucker, D. B., Belokurov, V., Evans, N. W., et al. 2006, *ApJ*, 643, L103

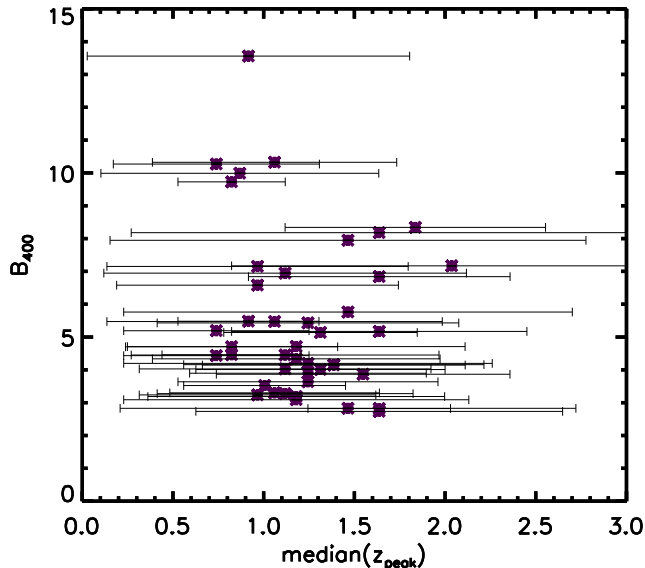


Figure 6. Subhalo concentration distributions (B_{400}) plotted as a function of z_{peak} , the median redshift at which V_{peak} is attained for each subhalo system. This is analogous to comparing B_{400} to the median infall time of each subhalo set. The error bars show the 1σ spread around the median value of z_{peak} for each subhalo set. There is no evident correlation, and we are also unable to find a correlation with any property of the main halo (e.g., concentration, mass, or formation time.)

APPENDIX

It is reasonable to expect the concentration factor, B_{400} , to be correlated to with some property of host halo. For example, the concentrations of dark matter halos are known to be correlated with formation redshifts (Navarro et al. 1997; Bullock et al. 2001). We have searched for relationships between B_{400} and several properties of the host halo, including virial mass, virial radius, R_{max} , V_{max} , and $M(< R_{\text{max}})$, but were unable to find any correlations. Figure 6 illustrates one such null result: B_{400} is plotted as a function of the median (asterisks) and 68% spread (error bars) in a_{peak} , the expansion factor at which a subhalo reaches V_{peak} , for each ELVIS halo. While the spread in a_{peak} is large for each system, there is no correlation with B_{400} .

Figure 7 explores a few different ideas for associating subhalos with bright satellites and the effect of that selection on their radial distributions. Specifically, for each of our 44 hosts we plot the implied B_{400} (puffiness) parameter (Equation 2) derived for three different choices of subhalo selection: the thirty highest V_{peak} (black, fiducial); the 30 highest V_{max} (magenta); and the 30 highest z_{peak} (cyan; defined as the redshift where V_{peak} was reached). We see that by selecting on z_{peak} we produce distributions that are not as puffy as our fiducial choice, and marginally consistent with the B_{400} of the MW, which is 1.7. However, subhalos chosen in this manner are an odd subset in terms of their mass. Figure 8 shows the V_{peak} and V_{max} mass functions of one example system selected in this manner (dashed) compared to all of the subhalos associated with this host (solid). It would demand a large number of $V_{\text{peak}} > 30\text{km s}^{-1}$ and $V_{\text{max}} > 20\text{km s}^{-1}$

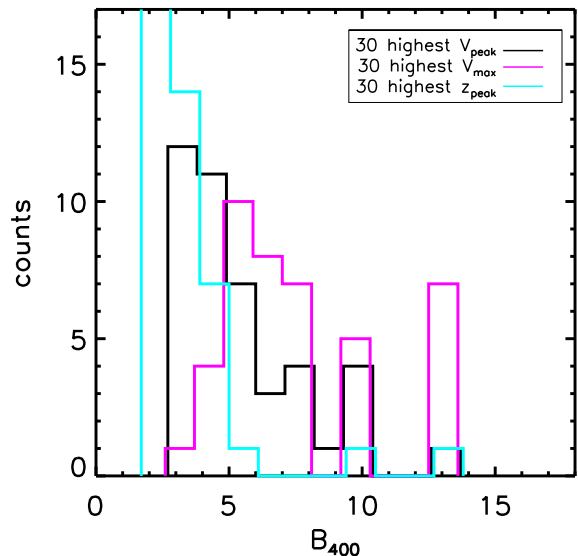


Figure 7. A histogram of B_{400} values for all 44 host halos computed by selecting the subhalos with the highest V_{peak} (black), V_{max} (magenta) and z_{peak} (cyan). The range and distribution of B_{400} depend somewhat on how subhalos are selected. Our selection of subhalos with the 30 highest V_{peak} predicts somewhat more concentrated distributions of satellites than does the selection based on V_{max} . The most concentrated distributions are found when selecting based on the earliest forming (highest z_{peak}) subhalos.

subhalos be dark. Such a model would be very difficult to understand from a galaxy formation perspective, as there is no obvious mechanism for allowing galaxies to form in halos of 30 km s^{-1} while suppressing galaxy formation in halos of $30 - 50\text{ km s}^{-1}$. Moreover, the choice amounts to selecting subhalos that reached their peak V_{max} value at redshifts between 2 and 4, well later than the epoch of reionization, which might offer more obvious channels for galaxy suppression mechanisms.

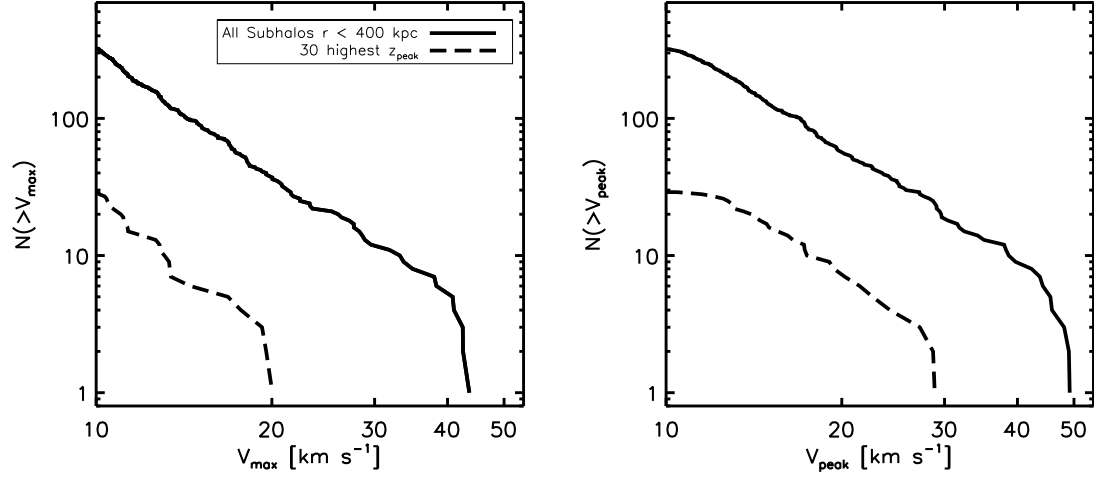


Figure 8. Cumulative counts of subhalos as a function of V_{max} (left) and V_{peak} (right) in a representative simulated halo. The solid lines correspond to all subhalos within 400 kpc of host halo, while the dashed lines represent a subset of those halos with the highest values of z_{peak} , the redshift at which the subhalo reached the V_{peak} . The ~ 10 most massive subhalos have $V_{\text{peak}} \gtrsim 40 \text{ km s}^{-1}$ or $V_{\text{max}} \gtrsim 30 \text{ km s}^{-1}$, whereas the ~ 10 largest early forming subhalos have $V_{\text{peak}} \gtrsim 18 \text{ km s}^{-1}$ or $V_{\text{max}} \gtrsim 12 \text{ km s}^{-1}$.